Recombination Controlled Signal Transfer through Mesoporous TiO_2 Films

Sven Rühle*,†,§,‖ and Thomas Dittrich‡,⊥

Department of Materials & Interfaces, Weizmann Institute of Science, Rehovot 76100, Israel, and Hahn-Meitner Institut, Glienicker Str. 100, 14109 Berlin, Germany

Received: September 14, 2005; In Final Form: November 23, 2005

Photocurrent transients were used to investigate electron transport in mesoporous, nanocrystalline TiO_2 films immersed into aqueous electrolyte, a regime where recombination cannot be neglected. Laser intensity and potential-dependent measurements show a decreased transient time of the current peak, which is explained by trap filling and electron loss from trap states into the electrolyte. A strongly enhanced recombination is furthermore observed, when the pH of the electrolyte is increased, while the current peak shifts toward longer transient times. Numerical simulations were used to decouple the impact of recombination and trapping on the transient response. We show that enhanced recombination in the absence of trapping accelerates the transfer of a current signal, while increased recombination slows down the transient current in the presence of electron trap sites.

Introduction

Porous films consisting of semiconducting nanoparticles with a wide electronic band gap such as TiO_2, ZnO, SnO_2, and Nb_2O_5 are of increasing technological interest.[1−5] Deposited onto a conducting substrate, such films are used as electrodes in photoelectrochemical solar cells such as the dye-sensitized solar cell (DSSC), in solid-state nanocomposite solar cells where a hole conductor replaces the electrolyte, as sensors or for catalytic applications. Electron transport within mesoporous films is fundamentally different from the transport properties in the bulk of such semiconductors, especially when they are immersed into electrolyte.[6] Due to the small dimensions of the interconnected nanocrystals, electrons always move close to the phase boundary between the semiconductor and the electrolyte. Electronic gap states, located at the electrolyte interface, can act as electron traps and recombination centers, which are slowing down electron transport and increase recombination.

Time-resolved photocurrent measurements are a powerful tool to investigate electron transport in porous films. The measurements are based on a laser-induced excitation profile of electrons and holes in the semiconductor.[6−19] Usually, holes are immediately injected into the electrolyte, and a strong nonuniform electron profile remains in the semiconducting network, which starts to propagate. Electric fields can be present very close to the substrate/TiO_2 interface,[20−23] while the main part of the film is practically field-free due to screening of the electrolyte. Exceptions are films with a strong nonuniform electron accumulation profile,[24,25] which are not considered here. Thus, electron transport is driven by diffusion,[6−8,12] which is strongly slowed by multiple trapping and detrapping events. Photocurrent transients can be used to determine an effective diffusion constant D_{eff} from the transient peak time t_p and the film thickness L:

$$D_{\text{eff}} = \frac{L^2}{6t_p} \tag{1}$$

This requires that electron recombination into the electrolyte is negligible and that the electrons are generated within a very thin layer at the electrolyte side of the TiO_2 film.[12]

In this work we present photocurrent transients measured on mesoporous TiO_2 films which are immersed into aqueous electrolyte. The experiments are performed at different illumination intensities, electrostatic potentials, and pH values of the electrolyte. Under such experimental conditions, recombination cannot be neglected, and simple analytical expressions such as eq 1 cannot be used for analysis. Numerical simulations are needed to investigate the impact of strong recombination and dispersive transport (e.g., trapping/detrapping) on the transient shape and current peak. We show that electronic gap states have opposite effects on the transient peak time, depending on whether they act more as electron traps or as recombination centers. Characteristic features in the experimental results are attributed to combined recombination−dispersion effects.

Experimental Methods

TiO_2 films were deposited onto conducting F-doped SnO_2 (FTO)-covered glass substrates (TEC 8 from Pilkington, 8 Ω/square sheet resistivity). Mesoporous TiO_2 films were produced by screen printing of a paste of TiO_2 nanoparticles, with an average diameter of 25 nm (Degussa P25). To prepare the paste, P25 powder was dissolved in acetic acid (pH 2) and kept for several minutes in ultrasound to break P25 aggregates. Carbowax was added to avoid cracks in the films. TiO_2 films were deposited onto the FTO substrate by screen printing, where an adhesive tape was used as a spacer. After drying in air, an interconnected network of TiO_2 nanoparticles was formed by annealing (at 250 °C for 30 min) and subsequent sintering in air (at 450 °C for 30 min) before the films were cooled within

* Corresponding author.
† Weizmann Institute of Science.
‡ Hahn-Meitner-Institut.
§ Current address: Condensed Matter & Interfaces, Debye Institute, University Utrecht, 3508 TA Utrecht, The Netherlands.
‖ E-mail: S.Ruhle@phys.uu.nl.
⊥ E-mail: dittrich@hmi.de.

10.1021/jp055196+ CCC: $33.50
Published on Web 02/08/2006

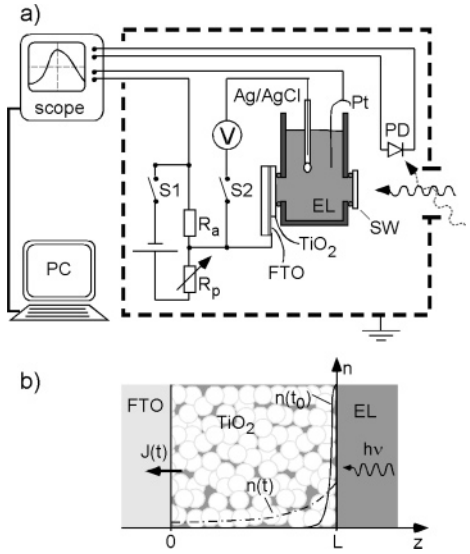

Figure 1. (a) Schematic drawing of the experimental setup. (b) Magnification of the mesoporous TiO_2 film immersed in electrolyte. Electron density profiles at t_0, immediately after laser excitation, and at some time $t > t_0$.

2−3 h to room temperature. The TiO_2 films are slightly n-type due to oxygen vacancies and have a thickness of 5 μm, which was determined from SEM cross-section measurements.

Transient measurements were performed in a homemade electrochemical cell (schematically shown in Figure 1), which was electrostatically screened by a Faraday cage (dashed line). The samples were sealed with an O-ring. When the switch S1 was closed, potentials between −0.2 and +0.9 V (measured through a voltmeter with an internal resistor of 10 MΩ) could be applied with respect to a calibrated Ag/AgCl reference electrode (Ag in saturated KCl solution). This was done by a potential divider with a fixed resistor R_a (50 Ω) and variable resistors R_p and by switching the polarity of a battery. During the transient measurements the switch S2 was kept open to avoid parasitic current through the reference electrode. A Pt counter electrode close to the sample surface was used to close the electrical circuit. Photocurrent measurements were carried out in 0.5 M, aqueous NaCl electrolytes (EL). The pH of the electrolyte was adjusted between 1 and 7 by adding drops of NaOH or HCl.

The samples were illuminated by pulses of a Nd:YAG-laser (wavelength 355 nm, duration time 150 ps, repetition rate 1 Hz) from the electrolyte side to generate electron−hole pairs within the mesoporous film (schematically shown in Figure 1b). The laser beam entered the electrochemical cell through a scattering window (SW) to excite homogeneously the TiO_2 film surface. The laser power was tunable from 0.11 to 3.76 mJ/pulse and the exposed surface area was approximately 0.6 cm^2, so that excitation intensities in the range from 0.18 to 6.27 mJ/cm^2 per pulse could be used.

Photocurrent transients were recorded with an oscilloscope (Hewlett-Packard, 54510B, 1-MΩ input resistance), which was externally triggered by a photodiode (PD) and controlled by a computer (PC). Low transient currents (all measured currents were in the sub-micro Ampère regime, see below) and thus low potential deviations during a transient measurement allowed us to use such a simple measurement configuration (for higher transient currents a potentiostat with a sufficient fast response has to be used). Prior to each measurement, the films were exposed to 10−20 laser flashes before each transient was recorded 10 times and averaged to obtain a well-stabilized signal.

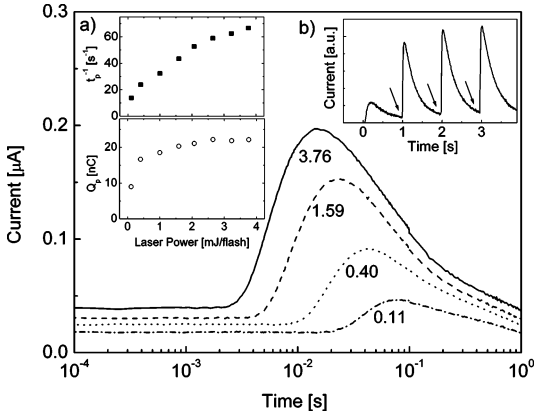

Figure 2. Photocurrent transients, recorded at excitation intensities of 0.11, 0.40, 1.59, and 3.76 mJ/pulse. (Inset a) The inverse transient peak time and the integrated peak charge as a function of the excitation energy. (Inset b) The first four transients prior to a measurement.

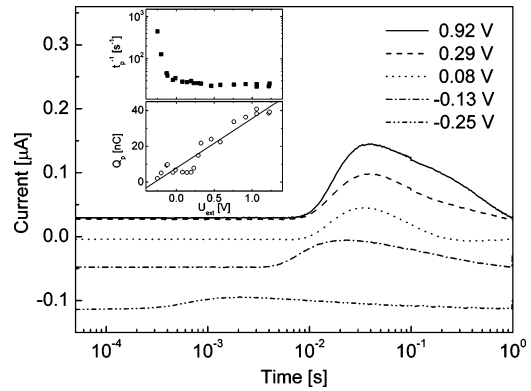

Figure 3. Transients, recorded at different electrostatic potentials, measured with respect to an Ag/AgCl reference electrode. The inset shows the inverse peak time and the integrated peak charge as a function of the applied potential. The straight line is a linear least-squares fit.

Results and Discussion

Photocurrent transients as a function of the incident laser intensity, measured with an electrolyte of pH 1, are shown on a logarithmic time scale in Figure 2. The laser intensity was varied from 0.11 to 3.76 mJ per laser pulse. With increasing laser intensity, a clear shift of the current peak toward shorter times was observed. Figure 2, inset a, shows the inverse transient peak time ($1/t_p$) and the integrated peak charge (Q_p) as a function of the excitation intensity, which both increase monotonically with increasing light intensity. While Q_p saturates at higher intensities, no such effect can be observed for $1/t_p$. Furthermore, one observes an increase of the steady-state offset current that is due to the periodic laser excitation of 1 Hz, which is required for good reproducibility of the measurements. As a consequence, the system cannot return into thermal equilibrium between consecutive pulses. Figure 2, inset b, shows the initial four transients measured at an illumination intensity of 0.4 mJ without pre-exposure. The amplitude of each transient rises until it converges to a constant value due to trap filling while the transient current does not decay entirely to zero within one second, such that the transient curves are superimposed to a small offset current (see arrows at the end of each transient).

Figure 3 shows measurements that were recorded at potentials from −0.25 to 0.92 V applied to the FTO substrate and measured with respect to an Ag/AgCl reference electrode. The

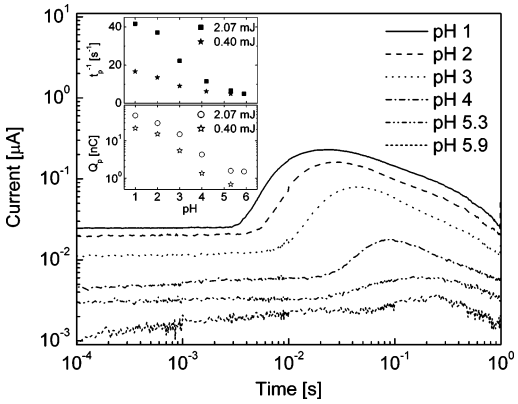

Figure 4. Measured photocurrent transients at different pH values of the electrolyte, plotted on a logarithmic current scale. The inset shows the inverse peak time and the integrated peak charge as a function of the pH value.

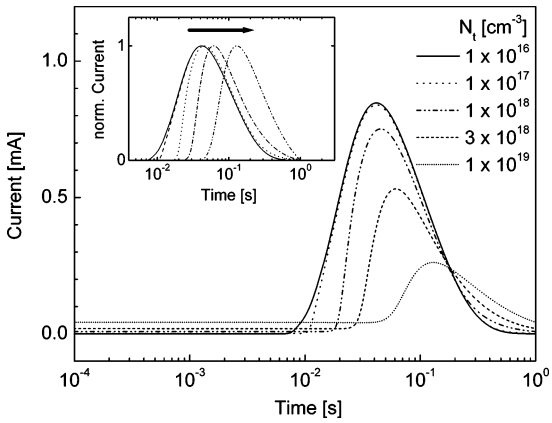

Figure 5. Simulated photocurrent transients, calculated for dispersive transport ($D = D(n)$) and trap densities ranging from 10^{16} to 10^{19} cm^{-3} in the absence of recombination.

(dark) open circuit potential (OCP) in thermal equilibrium was approximately 0.45 V, and the transients were measured in an electrolyte of pH 1 and a laser intensity of 0.4 mJ per pulse. Upon negative applied potential, a strong shift of the transient peak toward shorter times is observed while Q_p decreases. The inset shows that $1/t_p$ decreases by approximately 1 order of magnitude at negative potentials while Q_p is decreasing linearly when the applied potential is decreased. The offset current is positive for potentials around the OCP and more positive potentials; it is negative for potentials below ~0.05 V. A positive offset current is due to incomplete relaxation, as explained above, while electron transfer from the FTO into the TiO_2 and the electrolyte at negative applied potentials causes a negative background current.

Photocurrent transients as a function of the pH of the electrolyte were performed at a laser intensity of 0.40 and 2.07 mJ per pulse; the latter measurements are shown in Figure 4. The transient intensity depends strongly on the pH value of the electrolyte (note that the current is also plotted on a logarithmic scale). It decreases strongly with increasing pH value, while t_p shifts toward longer times. The inset shows the decrease of $1/t_p$ and Q_p with increasing pH value of the electrolyte. The strong decrease of Q_p indicates that electron recombination into the electrolyte is strongly enhanced at less acidic electrolytes. At pH values above 6 it was not possible to monitor transients above the noise level.

In the following, numerical simulations are used to investigate the effect of electron trapping/detrapping and recombination on photocurrent transients. Details about the simulation program are given in the Appendix so that it is only briefly described here. Electronic trap states were implemented into the program by an effective electron diffusion coefficient, which depends on the local electron density n and the trap density N_t, defined in eq A5 of the Appendix. Electron recombination from the TiO_2 into the electrolyte was implemented according to eq A6, where the order of the recombination mechanism was defined by a recombination exponent kp. The program allowed the implementation of experimental details such as periodic excitation and pre-exposure with several laser pulses. The input parameters for all numerical simulated transient curves are summarized in Table 1.

Dispersive Transport. The impact of electronic trap states on the transient current is shown in Figure 5 when recombination is neglected. A photocurrent transient in the absence of trap states ($D_{eff} = D_{CB}$) is shown as solid line, while the other transients were calculated for different trap densities N_t, according to eq A5. One can see that an increasing trap density decreases the peak current and causes an asymmetric shape of the transient curve on the logarithmic time scale. A shift of the current transient toward *longer* times can be seen from normalized curves shown in the inset. Furthermore the offset current increases as a result of the periodic excitation (Figure 5 shows the simulated current transient for the 10th laser pulse). Filled traps cannot be emptied between consecutive pulses so that the electron density remains above the thermal equilibrium concentration which results in a steady-state offset current. A difference of approximately 4 orders of magnitude between simulated and experimental transient currents indicates that in the measurements only a small fraction of electrons reaches the FTO substrate due to strong recombination into the electrolyte. In the following, the impact of recombination on the transient current is analyzed.

Recombination. Simulated photocurrent transients with different electron recombination rates k_n are shown in Figure 6, while the inset shows the same curves normalized to its peak current. For the simulations it was assumed that the diffusion coefficient is independent of the local electron concentration (nondispersive transport, $D_{eff} = D_{CB}$). The intensity of the transient current obviously decreases strongly with increasing recombination. We observe again that the simulated transient current at low recombination rates is orders of magnitude larger compared to the experiments (Figures 2−4), indicating that strong electron transfer into the electrolyte occurred during the measurements. The shape of the simulated transients does not change significantly, only the width of the transient peaks (on a logarithmic time scale) decreases at higher recombination rates,

TABLE 1: Parameters Used for Numerical Simulations

figure	5	6	7	8
D_{CB} [cm^2/s]	10^{-6}	10^{-6}	3×10^{-3}	3×10^{-3}
N_t [cm^{-3}]	see figure legend	0	10^{21}	10^{21}
k_n	0	see figure legend	3×10^{-16} cm^3/s	see figure legend
kp		1	2	2
I_{Laser}	0.40 mJ	0.40 mJ	see figure legend	2.07 mJ
L_{TiO_2} [μm]	5	5	5	5

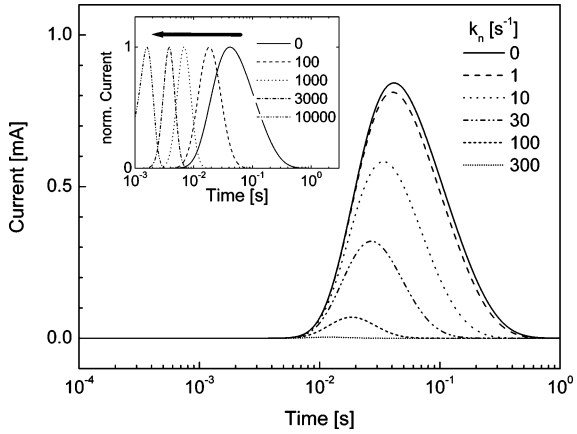

Figure 6. Simulated photocurrent transients for different recombination rate constants k_n in the absence of dispersive transport. The inset shows the same curves normalized to the peak current, which show a peak shift toward *shorter* times with increasing recombination.

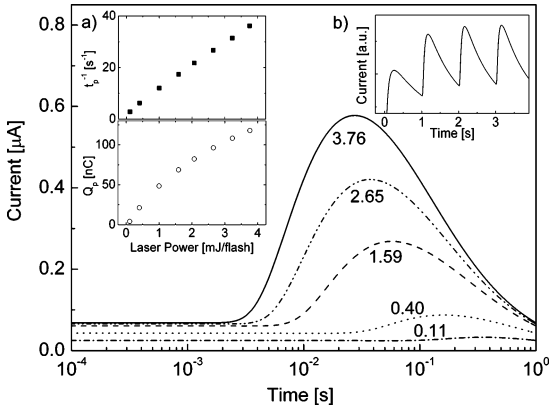

Figure 7. Photocurrent transients in the presence of recombination and dispersive transport, simulated for different laser powers (analogue to the experiments shown in Figure 2). The inset shows Q_p and $1/t_p$ as a function of the laser energy.

which can be seen from the inset. The important finding is a peak shift toward *shorter* times with increasing recombination, which means that the transfer of a pulsed current signal through a mesoporous film is strongly accelerated in the presence of large electron recombination into the electrolyte. We emphasize that the diffusion velocity of electrons is unaffected by recombination (the diffusion coefficient remains constant at all times), only the group velocity of a current pulse is accelerated. This has an important consequence: it is *not* possible in the presence of strong recombination to derive the correct electron diffusion constant from t_p according to eq 1. For the determination of the true diffusion constant, recombination is a clear limitation of time-resolved transient measurements.

Dispersive Transport with Recombination. The simulations above show that an asymmetric shape of the transient curve (on a logarithmic time scale) is an indication for dispersive transport. Furthermore, dispersive transport shifts the transient peak toward longer times with increasing trap density, while an opposite trend is observed when the recombination rate increases. In real experimental systems it is mostly not possible to separate the effect of trapping/detrapping and recombination—electron recombination into the electrolyte often goes through trap states at the semiconductor surface. Therefore the following simulations include recombination and dispersive transport caused by trapping/detrapping, and we will relate them to the experimental results. To achieve good agreement with measured transient curves we included a RC constant into the simulations shown in Figures 7 and 8, as described in the Appendix. We emphasize that the RC constant affects position and size of the transient peak,[18,19] but not the basic trend of Q_p or t_p.

Figure 7 shows a series of photocurrent transients calculated for different laser excitation energies with a second-order recombination mechanism ($kp = 2$). One can see that all experimental observed characteristic features such as the shift of t_p and the signal onset toward shorter times as well as a shift of the offset current can be simulated in good qualitative agreement with the measurements. Also the magnitude of the transient current is in good agreement with the experiments. The inset shows $1/t_p$ and Q_p as a function of the laser intensity, which exhibit a trend similar to that of the experiments (compare inset of Figure 2). The decreasing slope of Q_p as a function of excitation power is due to recombination that depends quadratic on the electron density (eq A6 with $kp = 2$), even though one can see that Q_p does not saturate. This indicates that the recombination in the experiments increases more strongly at

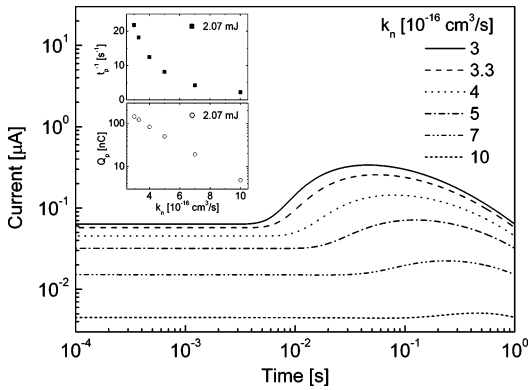

Figure 8. Simulated photocurrent transients for different recombination constants k_n in the presence of trap states N_t. Comparison with Figure 4 shows good agreement of the transient shape as well as the trend of Q_p and $1/t_p$, shown in the inset.

higher laser intensities (and thus at higher electron densities in the porous film) than described by the quadratic term in eq A6. Increased recombination at high electron densities can also be observed in potential dependent measurements, where Q_p decreases at more negative potentials. The simulations further show the successive filling of trap states within the first four laser flashes that leads to an initial increase of the transient intensity, which is shown in Figure 7, inset b.

Figure 8 shows a series of transients at different recombination rate constants for a system with dispersive transport due to trapping/detrapping. With increasing recombination, t_p shifts toward longer times in contrast to the trap-free case, shown in Figure 6. The inset shows the decrease of $1/t_p$ and Q_p with increasing recombination. Comparison with Figure 4 shows that pH-dependent measurements can be well described by a pH-dependent recombination rate constant in the presence of electron traps in the mesoporous film.[26]

Experiments and simulations show the big importance of the TiO_2 surface pH for electron recombination. For technical applications such as nanocomposite solar cells, based on mesoporous TiO_2 films, this is of particular importance because low recombination rates are desired for high-efficiency devices. Even though big efforts are currently made to replace the liquid electrolyte by a solid-state hole conductor, it should be kept in mind that a change of the surface pH during any fabrication step can have a huge impact on the recombination and thus the cell performance. The second technically relevant effect is the strong impact of the recombination on the transient time of a

pulsed current signal through such films, which could be used for sensor applications. Our simulations show that the signal transfer can be accelerated by recombination, if no electron traps are present in the film, or delayed, if electron transport is governed by trapping and detrapping events.

Conclusions

Photocurrent transients measured in aqueous electrolyte as a function of the electrostatic potential, the pH value of the electrolyte, and the laser intensity show a shift of the transient peak at negative applied potential and at high laser intensities, which is well explained by trap filling. Measurements at different pH values show a strong decrease in the transient current with increasing pH value and a delay in the transient peak. Numerical simulations suggest that electron recombination is increased in less acidic electrolytes. We have furthermore shown that enhanced recombination can accelerate the propagation of electronic signals through porous, nanocrystalline films, even though the diffusion coefficient remains constant. Characteristic features of measured transient curves in the strong recombination regime can be attributed to combined trapping/detrapping and recombination effects.

Acknowledgment. S.R. acknowledges the financial support provided by the Minerva Foundation (Munich) and the G.M.J. Schmidt Minerva Center for Supramolecular Chemistry. T.D. and S.R. acknowledge financial support from the European Union's Human Potential Program under Contract HPRN-CT-2000-00141, ETA Solar Cells, as well as fruitful scientific discussion within this framework, especially with C. Grasso and K. Fredin. The authors thank Prof. A. Zaban and his group for help in sample preparation.

Appendix A

For numerical simulations the mesoporous film of thickness L was divided into a discrete number of slices with constant thickness δz, where the slice index j is increasing from the substrate toward the electrolyte side of the film. The electron density n within the jth slice at the time t_k was calculated according to the one-dimensional, discretized continuity equation

$$n_j(t_k) = \left[\frac{1}{q}\frac{(J_{j+1/2}(t_{k-1}) - J_{j-1/2}(t_{k-1}))}{\delta z} - R_j(t_{k-1}) + G_j(t_{k-1})\right](t_k - t_{k-1}) + n_j(t_{k-1}) \quad \text{(A1)}$$

where G and R are electron generation and recombination, respectively. The current density J is defined between two neighboring slices,

$$J_{j+1/2} = qD_{j+1/2}\frac{n_{j+1} - n_j}{\delta z} \quad \text{(A2)}$$

The boundary conditions at the TiO_2/electrolyte side of the film were chosen as proposed by others.[6,13,27,28] Transient curves, shown in Figures 5 and 6, were calculated under the assumption of a perfect ohmic FTO/TiO_2 interface such that

$$J_{FTO} = J_{1/2} = D_{1/2}\frac{n_1 - n_0}{\delta z} \quad \text{(A3)}$$

where n_0 is the electron density in thermal equilibrium. For the simulations shown in Figures 7 and 8, the Helmholtz capacity C_{HL} of the FTO/electrolyte interface ($\sim 5\ \mu F/cm^2$) and the measurement resistor R_m of the oscilloscope (1 MΩ) were included. The Helmholtz capacitor is charged by J_{FTO} while electrons leave the capacitor through the scope according to

$$J_m = \frac{U_{HL}}{R_m A} = \frac{Q_{HL}}{R_m C_{HL} A} \quad \text{(A4)}$$

where U_{HL} is the potential drop across the Helmholtz layer, Q_{HL} is the accumulated charge in the Helmholtz layer, and A is the area of the FTO substrate in contact with the electrolyte (experimental conditions were chosen such that the illuminated TiO_2 area was identical with the geometric surface area in contact with the electrolyte, $A = 0.6\ cm^2$).

The impact of electronic trap states on the transient current was analyzed by a diffusion coefficient, similar to ref 6, that depends on the local electron density and the density of trap sites N_t:

$$D_{j+1/2} = \left(\frac{n_{j+1/2}}{N_t}\right)D_{CB} \quad \text{for } n_{j+1/2} < N_t \quad \text{(A5a)}$$

and

$$D_{j+1/2} = D_{CB} \quad \text{for } n_{j+1/2} \geq N_t \quad \text{(A5b)}$$

with

$$n_{j+1/2} = \frac{n_j + n_{j+1}}{2} \quad \text{(A5c)}$$

D_{CB} is the diffusion constant of conduction band electrons in the absence of trap states. The recombination rate (the loss of electrons from the TiO_2 film into the electrolyte) was defined as

$$R_j = k_n(n_j - n_0)^{kp} \quad \text{(A6)}$$

and depends on the electron density n_j within the jth slice, the recombination rate constant k_n, and a recombination exponent kp. The electron density at thermal equilibrium is labeled as n_0.

Generation of electrons in the TiO_2 film is due to electron−hole generation from super band gap illumination of a pulsed laser. Holes are much faster transferred into the electrolyte than electrons such that an excess electron density remains in the TiO_2 film. For the simulations it was assumed that the holes are removed instantaneously after laser excitation, and the electron generation rate was defined by

$$G_j(t_k) = \frac{I_{Laser}}{A\,\delta z}\frac{\lambda}{hc}B\exp(-\alpha(L - j\,\delta z)) \quad \text{for } t_k = 0\text{ s, }1\text{ s, }2\text{ s, ...} \quad \text{(A7a)}$$

and

$$G_j(t_k) = 0 \quad \text{for all time step iterations between the laser flashes} \quad \text{(A7b)}$$

The laser intensity is defined by I_{Laser} and is given in units of mJ. A is the area of the expanded laser beam, hc/λ is the energy of a single photon of wavelength λ, and B is the normalization constant ($B = (\sum_j \exp(-\alpha(L - j\,\delta z)))^{-1}$). The absorption coefficient is given by α and the TiO_2 film thickness is L, while the distance of the jth slice from the FTO substrate is $j\,\delta z$.

References and Notes

(1) Lenzmann, F.; Krüger, J.; Burnside, S.; Brooks, K.; Grätzel, M.; Gal, D.; Rühle, S.; Cahen, D. *J. Phys. Chem. B* **2001**, *105*, 6347.
(2) O'Regan, B.; Grätzel, M. *Nature* **1991**, *353*, 737.

(3) Keis, K.; Bauer, C.; Boschloo, G.; Hagfeldt, A.; Westermark, K.; Rensmo, H.; Siegbahn, H. *J. Photochem. Photobiol. A* **2002**, *148*, 57.
(4) Chappel, S.; Chen, S. G.; Zaban, A. *Langmuir* **2002**, *18*, 3336.
(5) Tennakone, K.; Bandara, J.; Bandaranayake, P. K. M.; Kumara, G. R. A.; Konno, A. *Jpn. J. Appl. Phys., Part 2* **2001**, *40*, L732.
(6) Cao, F.; Oskam, G.; Meyer, G. J.; Searson, P. C. *J. Phys. Chem.* **1996**, *100*, 17021.
(7) Duffy, N. W.; Peter, L. M.; Wijayantha, K. G. U. *Electrochem. Commun.* **2000**, *2*, 262.
(8) Kopidakis, N.; Benkstein, K. D.; van de Lagemaat, J.; Frank, A. J. *J. Phys. Chem. B* **2003**, *107*, 11307.
(9) Nakade, S.; Kubo, W.; Saito, Y.; Kanzaki, T.; Kitamura, T.; Wada, Y.; Yanagida, S. *J. Phys. Chem. B* **2003**, *107*, 14244.
(10) Nakade, S.; Saito, Y.; Kubo, W.; Kitamura, T.; Wada, Y.; Yanagida, S. *J. Phys. Chem. B* **2003**, *107*, 8607.
(11) Noack, V.; Weller, H.; Eychmüller, A. *J. Phys. Chem. B* **2002**, *106*, 8514.
(12) Solbrand, A.; Lindström, H.; Rensmo, H.; Hagfeldt, A.; Lindquist, S. E.; Södergren, S. *J. Phys. Chem. B* **1997**, *101*, 2514.
(13) Solbrand, A.; Henningsson, A.; Södergren, S.; Lindström, H.; Hagfeldt, A.; Lindquist, S. E. *J. Phys. Chem. B* **1999**, *103*, 1078.
(14) Solbrand, A.; Keis, K.; Södergren, S.; Lindström, H.; Lindquist, S.-E.; Hagfeldt, A. *Solar Energy Materials and Solar Cells* **2000**, *60*, 181.
(15) Weller, H.; Hoyer, P. *J. Phys. Chem.* **1995**, *99*, 14096.
(16) Kopidakis, N.; Schiff, E. A.; Park, N. G.; van de Lagemaat, J.; Frank, A. J. *J. Phys. Chem. B* **2000**, *104*, 3930.
(17) van de Lagemaat, J.; Frank, A. J. *J. Phys. Chem. B* **2001**, *105*, 11194.
(18) Schwarzburg, K.; Willig, F. *J. Phys. Chem. B* **2003**, *107*, 3552.
(19) Schwarzburg, K.; Ernstorfer, R.; Felber, S.; Willig, F. *Coord. Chem. Rev.* **2004**, *248*, 1259.
(20) Kron, G.; Rau, U.; Werner, J. H. *J. Phys. Chem. B* **2003**, *107*, 13258.
(21) Rühle, S.; Cahen, D. *J. Phys. Chem. B* **2004**, *108*, 17946.
(22) Rühle, S.; Dittrich, T. *J. Phys. Chem. B* **2005**, *109*, 9522.
(23) Schwarzburg, K.; Willig, F. *J. Phys. Chem. B* **1999**, *103*, 5743.
(24) Lana-Villarreal, T.; Bisquert, J.; Mora-Seró, I.; Salvador, P. *J. Phys. Chem. B* **2005**, *109*, 10355.
(25) Vanmaekelbergh, D.; de Jongh, P. E. *J. Phys. Chem. B* **1999**, *103*, 747.
(26) It should be mentioned that the simulation program has several degrees of freedom (number of input parameters) such that more than one unique set of simulation parameters can be found to describe a certain effect. The impact of an increased trap density N_t on D_{eff} can, for example, be compensated by a bigger diffusion constant D_{CB}. The numbers given in Table 1 should be considered as reasonable material parameters and not as extracted fit parameters from measurements. However, this does not affect the discussed effects, which are valid for a huge range of reasonable input parameters.
(27) Nelson, J. *Phys. Rev. B* **1999**, *59*, 15374.
(28) Fredin, K.; Grasso, C.; Rühle, S.; Hagfeldt, A. *Sol. Energy Mater. and Sol. Cells*, in press.